Biophysical *Journal*
Article

Biophysical Society

Molecular Features of the Zn^{2+} Binding Site in the Prion Protein Probed by ^{113}Cd NMR

Kate A. Markham,[1] Graham P. Roseman,[1] Richard B. Linsley,[1] Hsiau-Wei Lee,[1] and Glenn L. Millhauser[1,*]
[1]Department of Chemistry and Biochemistry, University of California, Santa Cruz, Santa Cruz, California

ABSTRACT The cellular prion protein (PrP^C) is a zinc-binding protein that contributes to the regulation of Zn^{2+} and other divalent species of the central nervous system. Zn^{2+} coordinates to the flexible, N-terminal repeat region of PrP^C and drives a tertiary contact between this repeat region and a well-defined cleft of the C-terminal domain. The tertiary structure promoted by Zn^{2+} is thought to regulate inherent PrP^C toxicity. Despite the emerging consensus regarding the interaction between Zn^{2+} and PrP^C, there is little direct spectroscopic confirmation of the metal ion's coordination details. Here, we address this conceptual gap by using Cd^{2+} as a surrogate for Zn^{2+}. NMR finds that Cd^{2+} binds exclusively to the His imidazole side chains of the repeat segment, with a dissociation constant of ~1.2 mM, and promotes an N-terminal-C-terminal *cis* interaction very similar to that observed with Zn^{2+}. Analysis of ^{113}Cd NMR spectra of PrP^C, along with relevant control proteins and peptides, suggests that coordination of Cd^{2+} in the full-length protein is consistent with a three- or four-His geometry. Examination of the mutation E199K in mouse PrP^C (E200K in humans), responsible for inherited Creutzfeldt-Jakob disease, finds that the mutation lowers metal ion affinity and weakens the *cis* interaction. These findings not only provide deeper insight into PrP^C metal ion coordination but they also suggest new perspectives on the role of familial mutations in prion disease.

INTRODUCTION

Transmissible spongiform encephalopathies, also known as prion diseases, are a class of fatal neurodegenerative diseases for which there is no cure or treatment (1). Examples of prion diseases are Kuru and Creutzfeldt-Jakob disease (CJD) in humans, scrapie in sheep, chronic wasting disease in cervids, and mad cow disease (2). Prion diseases originate from genetic, sporadic, or infectious routes and involve misfolding of the predominately helical cellular prion protein (PrP^C) to the β-sheet rich scrapie form (2). Similar to Alzheimer's disease, sporadic disease accounts for the majority of prion cases in humans.

PrP^C is expressed throughout the body but appears to be concentrated primarily at pre- and postsynaptic neuronal membranes (3–5). The precise physiological function of PrP^C is largely unknown; however, the protein's well-documented ability to coordinate Cu^{2+} and Zn^{2+} suggests a role in metal ion homeostasis (6–10). Mature human PrP^C is a 208-amino-acid protein with two N-linked glycans and a glycophosphatidylinositol moiety that anchors the protein to the extracellular membrane surface. The protein has two distinct domains: the C-terminal domain (residues 126–230) composed of three α-helices, two short antiparallel β-strands, and a disulfide bond linking helices two and three and the N-terminal domain (residues 23–125), a flexible segment that coordinates both Cu^{2+} and Zn^{2+} in vivo (7,10–13).

Zn^{2+} is one of the most abundant trace metal in the brain with roles in diverse functions, including structural support in certain transcription factors, as catalytic elements in zinc metalloenzymes and as an abundant counterion in presynaptic glutamate vesicles (13,14). Glutamate release results in a synaptic (Zn^{2+}) spike, and recent findings suggest that Zn^{2+} binding to PrP^C stimulates Zn^{2+} transport back into neurons through α-amino-3-hydroxy-5-methyl-4-isoxazole-propionic acid (AMPA) receptors, thereby restoring normal synaptic metal ion concentrations (14). Our lab demonstrated previously that Zn^{2+} binds to a PrP^C N-terminal segment composed of the sequence $(PHGGGWGQ)_4$ (residues 60–91 in human PrP^C), termed the octarepeat (OR) domain, with a dissociation constant (K_d) of ~200 μM (Fig. 1) (10). This OR segment is essential for Zn^{2+} binding and subsequent transport of the ion through AMPA receptors.

Although once thought to be noninteracting, we recently demonstrated that PrP^C's N-terminal and C-terminal domains have an important interdomain interaction driven

Submitted August 24, 2018, and accepted for publication January 4, 2019.
*Correspondence: glennm@ucsc.edu
Editor: Wendy Shaw.
https://doi.org/10.1016/j.bpj.2019.01.005

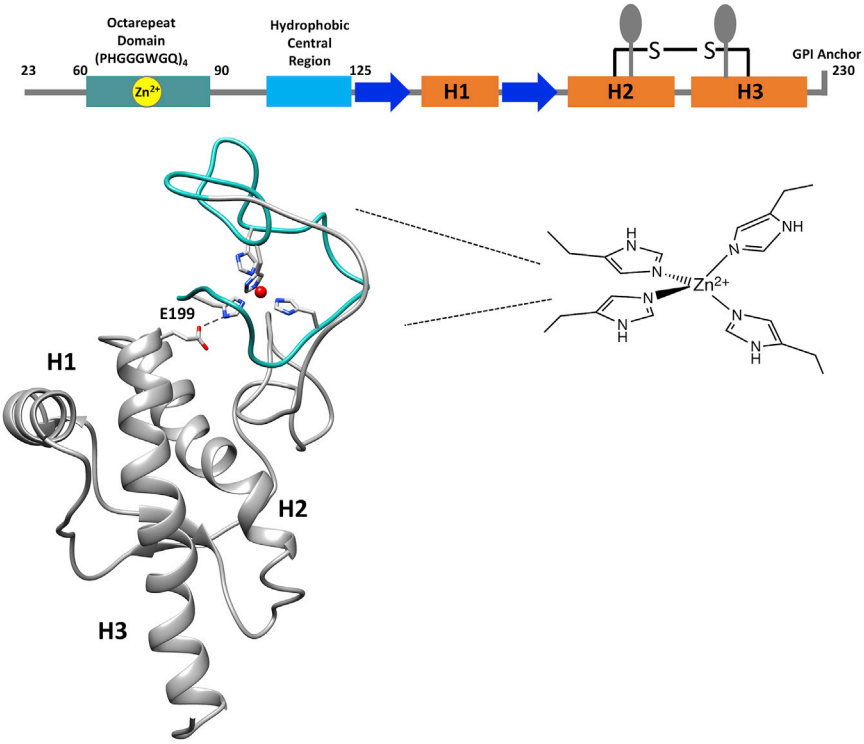

FIGURE 1 Sequence and structural model of mouse PrP^C-Zn^{2+} complex. (*top*) Linear sequence diagram of PrP^C(23–230) (mouse sequence) with numbering indicating important N-terminal segments, along with secondary structure and posttranslational modifications of the folded C-terminal domain. Coloring shows the octarepeat (OR) domain (*light green*) that coordinates Zn^{2+}, β sheets (*blue*), helices (*orange*), CR segment (*light blue*), glycans (*ovals*), disulfide bond linking helices two and three, and glycophosphatidylinositol anchor at residue 230. (*bottom*) Three-dimensional ribbon model of PrP^C with Zn^{2+} (*red sphere*) coordinated to the OR domain His residues and docked against a C-terminal cleft formed by helices 1–3 (Spevacek et al. (15)). Also shown is residue E199 (mouse sequence) with its carboxylate group forming a hydrogen bond with the remote NH of a coordinating His residue.

by the addition of physiological metal ions (6,7,15). Evidence for this *cis* interaction came from detailed double electron-electron resonance (DEER) EPR and ^{1}H-^{15}N heteronuclear single-quantum coherence (HSQC) NMR. Specifically, Spevacek et al. (15) demonstrated that the addition of Zn^{2+} drives the N-terminal OR to make a direct contact with a negatively charged patch on C-terminal surface composed of residues from helices two and three as well as the N-terminal end of the β1-α1 loop extending to the beginning of helix 1. Interestingly, a significant number of pathological mutations responsible for inherited prion disease reside on this surface, and those tested systematically weakened the observed *cis* interaction (15). Therefore, it was hypothesized that PrP^C's *cis* interaction plays a role in regulating the prion protein (PrP), with a decrease in this *cis* interaction promoting prion-mediated toxicity.

In addition to Zn^{2+}, Cu^{2+} also drives a *cis* interaction, as shown by Evans et al. (6). This was demonstrated using paramagnetic relaxation enhancement NMR and DEER EPR. Paramagnetic relaxation enhancement broadening of PrP^C ^{1}H-^{15}N HSQC NMR crosspeaks with 1.0 equivalent of Cu^{2+} localized the *cis* interaction to the same C-terminal PrP^C surface identified in the Zn^{2+} studies. The specific location of the Cu^{2+} ion was further refined using DEER-EPR-derived distance restraints, along with trilateration calculation (6). These structural data suggest that physiologically relevant metal ions are essential for stabilizing higher order structure in PrP^C. Recent monoclonal antibody and electrophysiology experiments underscore the importance of this newly discovered *cis* interaction (16). These experiments show consistently that the PrP^C C-terminal domain regulates the otherwise toxic N-terminal executive domain. Using mutagenesis and select PrP^C constructs, we have provided strong evidence that this regulatory function requires the Zn^{2+}/Cu^{2+}-promoted *cis* interaction identified by our magnetic resonance experiments (6,7,15–17).

Cu^{2+} is a paramagnetic species, which enables EPR experiments for assessing details of the metal ion's coordination environment. Using EPR with 1.0 equivalent of Cu^{2+}, we showed that the copper ion is bound to the four imidazole side chains of the OR histidines (9). This coordination environment is preserved in both the OR domain alone when expressed as a polypeptide as well as in the full-length protein. This information was essential in developing a structural model of Cu^{2+}-occupied PrP^C.

Unlike Cu^{2+}, there is no convenient magnetic resonance method for probing the coordination environment of Zn^{2+}. However, given the essential role of Zn^{2+} in PrP^C physiology, as evidenced by the ion's ability to trigger divalent ion transport through the AMPA receptor (14), it is very important to evaluate the precise details of how this physiological ion coordinates within PrP^C. We have shown previously with indirect methods such as mass spectrometry mapping applied to OR peptides that, much like Cu^{2+}, Zn^{2+} binds to the OR through imidazole coordination (10). However, this has yet to be demonstrated in the full-length PrP. As such, it is unclear whether Zn^{2+} remains

confined solely by the histidine residues of the OR segment or, alternatively, forms a direct bond to the C-terminal residue side chains.

To investigate the molecular details, we report here the application of ^{113}Cd NMR spectroscopy to probe Zn^{2+} coordination in PrP^C. Cd^{2+}, like Zn^{2+}, is a transition metal in group 12 of the periodic table and therefore forms a stable divalent ion with a diamagnetic d^{10} electron configuration (18). Being separated by just one period, the ionic radii of Cd^{2+} and Zn^{2+} are similar at 0.98 and 0.74 Å, respectively (18). As demonstrated in the context of other proteins, Cd^{2+} is an excellent Zn^{2+} surrogate recapitulating zinc's coordination properties (19). For example, the zinc metalloenzymes carbonic anhydrase B and C were studied using ^{113}Cd NMR spectroscopy (20,21). The enzymes retained activity with Cd^{2+} at the catalytic center, and analysis of the ^{113}Cd NMR spectra distinguished between competing coordination models by identifying an exchangeable water molecule at the active site (22).

Cd has two spin-1/2 isotopes: ^{111}Cd and ^{113}Cd. Of these, ^{113}Cd is somewhat more sensitive and thus more desirable for NMR studies (23). ^{113}Cd NMR offers several advantages for probing metal ion binding sites (22,24,25). ^{113}Cd NMR signals are spread over a remarkably wide chemical shift range, ~900 ppm, with specific resonances sensitive to coordination geometry and specific coordinating atoms (23). ^{113}Cd chemical shifts are predictable with deshielding following the empirical relationship S > N > O (26–28). Consequently, ^{113}Cd NMR provides a sensitive probe for assessing the metal ion coordination environment. Although ^{113}Cd is a low-sensitivity nucleus, enrichment to 94.8% (natural abundance of ^{113}Cd is 12.26%) allows for acquisition of high-quality spectra in ~12 h using a broad-band, nitrogen-cooled cryoprobe on a ^{1}H 500-MHz instrument (corresponding to a ^{113}Cd resonance frequency of ~111 MHz) (29). Finally, because of the uniqueness of ^{113}Cd, spectra are devoid of background signals.

In this study, we use ^{1}H-^{15}N NSQC NMR to compare the interactions of Zn^{2+} and Cd^{2+} with PrP^C. Titration studies and $^2J_{NH}$ couplings from HSQC experiments are used to assess the Cd^{2+}-PrP^C K_d (30,31). Next, using ^{113}Cd NMR, we compare binding in the isolated OR domain and in the full-length protein. Finally, we evaluate PrP^C mutants relevant to prion toxicity and disease using both NMR and isothermal titration calorimetry (ITC). Together, these data advance the understanding of metal ion coordination in PrP^C and show, specifically, that 1) Cd^{2+} is an excellent Zn^{2+} surrogate and useful tool for probing the features of metal ion coordination in PrP^C, 2) Cd^{2+} binding in both the OR domain and full protein is dominated by His coordination and is spectroscopically equivalent, 3) a highly penetrant, familial, disease-associated mutant that alters C-terminal domain charge triggers a loss of metal ion binding affinity, and 4) basic residues of the C-terminal domain may stabilize the global PrP^C fold through hydrogen bonding to the metal ion coordinating His residues of the OR segment.

MATERIALS AND METHODS

^{15}N-labeled protein expression

PrP and its variants were constructed using the template plasmid pJexpress 414 mouse PrP (DNA 2.0) containing full-length *Mus musculus* PrP (23–230). All constructs and mutations were confirmed by DNA sequencing. Protein expression was carried out in *Escherichia coli* BL21Star (DE3) (Invitrogen, Carlsbad, CA). For ^{1}H-^{15}N HSQC NMR experiments, ^{15}N-labeled proteins were grown per the protocols reported by Evans et al. (6). N-terminal PrP (23–125) was produced by introducing a tobacco etch virus cleavage site to remove the C-terminal (126–230) domain (32).

Peptide synthesis

The linear peptide (referred to as the 4-Octa peptide or peptide) KKRPKPWGQPHGGGWGQPHGGSWGQPHGGSWGQPHGGGWGQ-NH_2, corresponding to KKRPKP-PrP(56–90)-NH_2, (molecular weight = 4291.66, ε = 28,450 $cm^{-1}M^{-1}$) was prepared by solid-phase peptide synthesis using standard fluorenylmethoxycarbonyl chemistry protocols on a Liberty 1 Microwave Peptide Synthesizer (CEM). 4-Octa peptide was cleaved from ChemMatrix Rink amide resin (Sigma Aldrich, St. Louis, MO) and purified by reverse-phase C18 high-performance liquid chromatography and lyophilized for long-term storage once it reached analytical purity.

NMR spectroscopy

PrP^C and PrP-derived peptide samples for ^{1}H-^{15}N NMR experiments were prepared at 300 μM protein or peptide in a buffer containing 10 mM 2-(*N*-morpholino)ethanesulfonic acid (MES; Sigma), 10% D_2O, at pH 6.0 or 7.0, depending on the specific experiment. Subsequent to the addition of 1.0 mM $CdCl_2$, the pH was measured and adjusted, if necessary. ^{1}H-^{15}N HSQC spectra were recorded at 25°C on an 800-MHz spectrometer (Bruker, Billerica, MA) at the University of California, Santa Cruz NMR facility (Santa Cruz, CA). NMR spectra were analyzed with NMRPipe (33) and Sparky. Structural analysis was performed with Chimera (34). Protein assignments were achieved using previously determined values from Evans et al. (6).

The Cd^{2+} K_d was determined from ^{1}H-^{15}N-HSQC spectra using nonlinear least-squares fitting to the following equation (35):

$$\Delta\delta_{obs} = \Delta\delta_{max}\left\{\left([P]_t + [L]_t + K_d\right) - \left[\left([P]_t + [L]_t + K_d\right)^2 - 4[P]_t[L]_t\right]^{\frac{1}{2}}\right\}\Big/2[P]_t,$$

where $[P]_t$ and $[L]_t$ are the total protein and ligand (Cd^{2+}) concentrations, respectively, and $\Delta\delta_{max}$, determined from the fitting procedure, is the difference in chemical shift between the free and fully bound protein.

For ^{113}Cd NMR experiments, all samples were prepared in buffer containing 10 mM MES buffer (Sigma), 10% D_2O at pH 6.0 and 25°C, with either 300 μM protein, EDTA or 1.8 mM imidazole, and 1.0 mM $^{113}CdCl_2$ (Cambridge Isotopes; 95% isotopically labeled). ^{113}Cd NMR acquisition was performed on the San Francisco State University Bruker AVANCE NEO 500 MHz (11.7 T) spectrometer, fitted with a nitrogen-cooled cryoprobe. The spectrometer was tuned to 110.9 MHz. All samples were externally referenced to 0.1 M $Cd(ClO_4)_2$ (aqueous [aq]).

Analysis leading to the conclusion of fast exchange in the ^{113}Cd spectra utilized the following relations:

$$P + L \underset{k_{off}}{\overset{k_{on}}{\rightleftharpoons}} P:L$$

$$K_d = \frac{k_{off}}{k_{on}}$$

$$k_{ex} = [P]k_{on} + k_{off}$$

$$\Delta\omega = 2\pi\Delta\delta\nu_o,$$

where $\Delta\delta$ is the difference in ^{113}Cd chemical shift between free Cd^{2+} and the fully bound metal ion, and ν_o is the spectrometer frequency. k_{on} is estimated to be diffusion controlled and $\sim 10^9$ $M^{-1}s^{-1}$. With a protein concentration of 300 μM, $k_{ex} >> \Delta\omega$ thereby satisfying fast exchange consistent with a single ^{113}Cd NMR line.

ITC

ITC experiments were conducted using a MicroCal VPITC calorimeter. Zinc chloride titrations were performed by adding 2.0 mM zinc chloride into each PrP^C construct (18–45 μM) at pH 7.4 in 50 mM 3-(*N*-morpholino)propanesulfonic acid (MOPS). Cadmium chloride titrations were performed by titrating 20 mM cadmium chloride into each PrP^C construct (45–60 μM) at pH 6.0 in 10 mM MES. Each construct was dialyzed overnight before running the experiments in either 50 mM MOPS pH 7.4 (Zn^{2+} titrations) or 10 mM MES pH 6.0 (Cd^{2+} titrations). Metal ions used in the titrations were prepared by diluting a 1.0 M stock in water to either 2.0 mM for zinc chloride or 20 mM for cadmium chloride using the MOPS or MES dialysis buffer, respectively. Because of the large heats of dilution with cadmium chloride, the integrated ITC data were background corrected. Data analysis was performed using the Origin calorimetry software package. Experiments were replicated two to three times for each construct, and the reported error is the difference between the highest and lowest K_d measured for each set of measurements.

RESULTS

Cadmium induces a *cis* interaction between PrP^C N-terminal and C-terminal domains

Previous ^{1}H-^{15}N HSQC NMR experiments performed on uniformly ^{15}N-labeled PrP^C with one to three equivalents of Zn^{2+} identified a collection of C-terminal residues that exhibited both linewidth broadening and/or changes in chemical shift of select crosspeaks. The affected residues, when mapped to the three-dimensional structure of the C-terminal domain of PrP^C, identified a shallow cavity localized primarily to a surface patch composed of adjacent sides of helices 2 and 3 (α2 and α3), along with the residues corresponding to the β1-α1 loop. When combined with EPR DEER experiments and suitable controls, these NMR data demonstrated that the Zn^{2+}-OR segment docks to a well-defined, negatively charged patch on the PrP^C C-terminal domain (Fig. 1) (15). Divalent Zn is diamagnetic; we therefore attributed changes in the line shapes and chemical shifts of the affected C-terminal residues to intermediate exchange molecular dynamics at the interface between the interacting N-terminal and C-terminal domains. To confirm the use of Cd^{2+} as a viable Zn^{2+} surrogate, we performed parallel ^{1}H-^{15}N HSQC NMR experiments at 25°C on ^{15}N-labeled wild-type PrP^C(23–230) (300 μM) in the presence of 1.0 mM Cd^{2+} (added as $CdCl_2$) at pH 6.0 and pH 7.0.

Fig. 2 *A* shows a segment of the 800-MHz ^{1}H-^{15}N HSQC NMR spectrum. As with Zn^{2+}, we find that select crosspeaks exhibit changes in linewidth and chemical shift (15). To evaluate these spectral changes, values for intensity ratio (I/I_o) were calculated for all assigned C-terminal resonances. These ratios are obtained by dividing the crosspeak intensity in the presence of Cd^{2+} by the intensity of the crosspeak before addition of Cd^{2+}. The average and SD of the I/I_o values were calculated, and standard Z-score analysis (6) was performed to determine a threshold for residues broadened more than 1.0 SD from the mean by the presence of Cd^{2+}. In addition, crosspeaks exhibiting changes in chemical shift greater than 0.1 ppm (measured by $[(\Delta\delta^1H)^2 + (\Delta\delta^{15}N/9)^2]^{1/2}$) were deemed to be significantly affected by the addition of Cd^{2+}. The results are summarized in Fig. 2 *B*, which shows I/I_o versus residue position for the C-terminal domain. Affected residue crosspeaks exceeding statistical significance are noted by dark blue (I/I_o exceeding one SD the mean), medium blue (I/I_o greater than 0.5 SD with a chemical shift change greater than 0.1 ppm), and in light blue (0.1 ppm or greater change in chemical shift) (6,35). When plotted onto surface (Fig. 2 *C*) or ribbon (Fig. 2 *D*) diagrams, the data identify a patch of affected residues similar to those observed by the addition of Zn^{2+}. Specifically, the Cd^{2+} caused either broadening, shifting or broadening and shifting of proximal residues on α2, α3, and the β1-α1 loop. The 27 affected residues are all proximal to each other and, of these, 12 are equivalent to those affected by Zn^{2+} (Fig. S1). Spectra acquired at pH 6.0 and 7.0 gave similar results; however, for experiments that follow, we standardized on the lower pH value because it was found to give narrower ^{113}Cd line shapes (see below, Fig. 5). Noting that Zn^{2+} does not bind to PrP^C(90–230), these results show that like Zn^{2+}, Cd^{2+} drives a well-defined *cis* interaction between the PrP^C Cd^{2+}-occupied N-terminal domain and the shallow cavity of the C-terminal domain.

Cd^{2+} coordinates to imidazole groups of OR histidines

We previously used chemical mapping to show that Zn^{2+} coordinates specifically to His imidazole residues in the PrP^C OR segment with a K_d of $\sim$200 μM (10). To examine Cd^{2+} coordination details and measure its binding affinity, we applied ^{1}H-^{15}N HSQC with pulse sequence modifications to highlight $^2J_{NH}$ scalar couplings (30). With this pulse

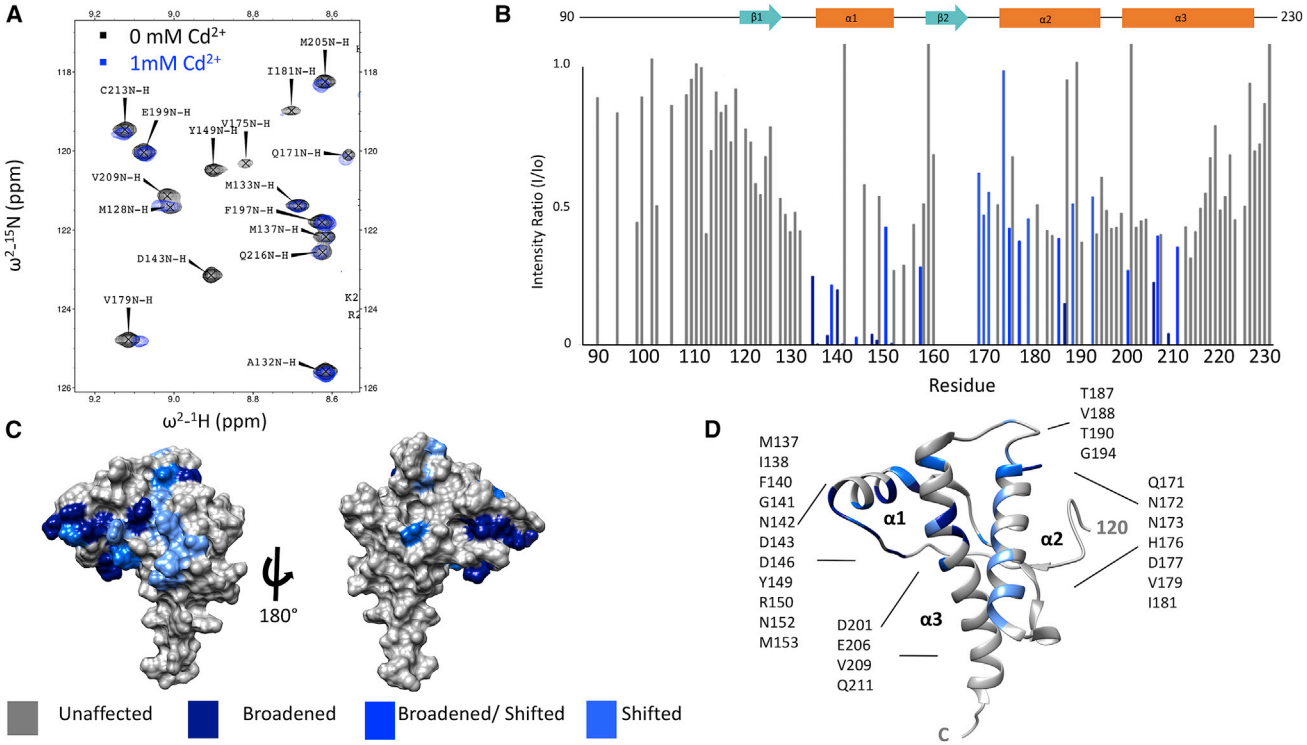

FIGURE 2 Cd^{2+} promotes an interdomain interaction wild-type PrP at pH 6.0. (*A*) A selected region of the ^{1}H-^{15}N HSQC of wild-type PrP in the absence of metal (*black*) and in the presence of 1.0 mM of Cd^{2+} (*blue*). (*B*) A bar graph of I/I_o for residues 90–23 of PrP^C in the presence of Cd^{2+}. (*C* and *D*) Surface and ribbon plots, respectively, of C-terminal residues affected by the presence of Cd^{2+} (coordinates from Protein Data Bank (PDB): 1XYX). Affected residues are noted specifically on the ribbon diagram.

sequence, His side chains give characteristic patterns depending on the protonation state of the imidazole ring. Spectra of full-length PrP^C and PrP (23–125), both in the absence of Cd^{2+}, are compared in Fig. 3. PrP^C contains 9 His residues, 6 of which are in the flexible region 23–125. Examination of Fig. 3 shows that Hε1 crosspeaks with ^{1}H chemical shifts above 8.1 ppm are readily assigned to this N-terminal segment. In addition, prominence of the specific crosspeak patterns of Nδ1-Hε1, Nε2-Hε1, and Nε2-Hδ2 for each imidazole is consistent with protonation of the ε2 nitrogen of the imidazole ring. Three separate patterns are observed for PrP (23–125) with approximate volume ratios of 4:1:1. We therefore assigned the four OR His residues to more intense set crosspeaks.

Next, we added increasing concentrations of Cd^{2+} to a solution of 300 μM PrP (23–125) and observed a progressive chemical shift changes of the Nε2-Hε1 and Nε2-Hδ2 crosspeaks, assigned to the OR His residues (Fig. 4). The peaks exhibited only slight broadening with increasing [Cd^{2+}], consistent with fast exchange. These data suggest that Cd^{2+} coordinates preferentially to the ε2 nitrogen, perhaps displacing the exchangeable proton. Plotting the Nε2 ^{15}N chemical shifts derived from the Nε2-Hε1 and Nε2-Hδ2 crosspeaks gave saturable binding curves, which we fit independently to a standard model for equilibrium fast exchange (35). Both curves gave similar results with an approximate K_d of 1.2 mM (Table 1). We also attempted titration with full-length PrP^C; however, the relevant $^{2}J_{NH}$ crosspeaks exhibited significant broadening, likely because of intermediate exchange, and were therefore not amenable to fast-exchange binding analysis. Taken together, these NMR

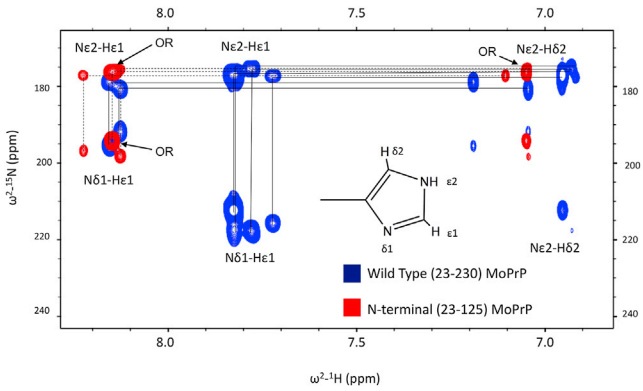

FIGURE 3 $^{2}J_{NH}$-HSQC of ^{15}N-labeled N-terminal PrP and full-length PrP^C. ^{1}H-^{15}N-HSQC spectra with pulse sequence modified to highlight $^{2}J_{NH}$ couplings showing the imidazole region of the spectrum for mouse PrP(23–125) (*red*, correlated crosspeaks connected by *dashed lines*) and full-length PrP (*blue*, peaks connected by *solid lines*). The pattern of connections from Nδ1-Hε1 → Nε2-Hε1 → Nε2-Hδ2 is characteristic of the protonation at Nε2. Crosspeaks from the octarepeat (OR) His residues are labeled "OR."

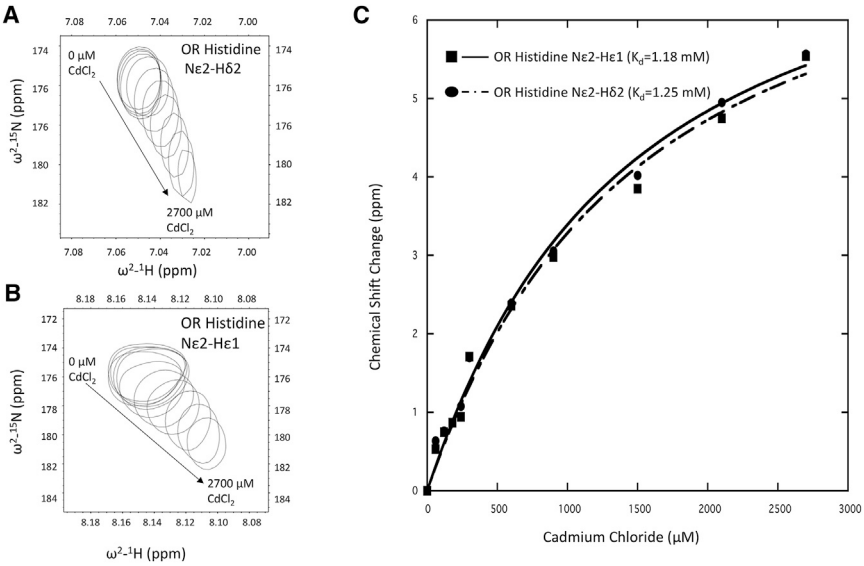

FIGURE 4 Determination of K_d from $^2J_{NH}$ HSQC chemical shifts versus Cd^{2+}. (*A*) Nε2-Hδ2 and (*B*) Nε2-Hε1 $^2J_{NH}$ HSQC crosspeaks of N^{15}-labeled PrP (23–125) shift as a function of added cadmium chloride. (*C*) A plot of ^{15}N chemical shift change versus $CdCl_2$. Data were fitted to the K_d expression derived for fast chemical exchange (Materials and Methods) to determine binding constant for Cd^{2+} to the OR domain (Table 1). Resulting K_d values derived from the Nε2-Hδ2 and Nε2-Hε1 crosspeaks are ~1.25 and 1.18 mM, respectively.

experiments demonstrate that Cd^{2+}, like Zn^{2+}, binds to the OR His residues but with a significant reduction in affinity.

^{113}Cd NMR of wild-type PrP^C and relevant mutants

With the goal of assessing the Cd^{2+} coordination environment, we carried out direct NMR measurements on ^{113}Cd combined with PrP^C and various relevant constructs. With an 11.7 T magnetic field (500 MHz for ^{1}H), the ^{113}Cd resonance frequency is 110.9 MHz (29). All spectra were referenced to the chemical shift of 0.10 M Cd $(ClO_4)_2$ (aq), which places the chemical shift of aquo ^{113}Cd at 0 ppm (29). Given the low gyromagnetic ratio of ^{113}Cd, it was essential to adjust sample conditions to give the best possible spectra. Consequently, we prepared peptides and proteins to concentrations of 300 μM, which is near the PrP^C solubility limit, along with 1.0 mM $^{113}CdCl_2$. Under these conditions, a spectrometer fitted with a cryoprobe was capable of acquiring resolvable spectra in approximately 12 h.

Resulting spectra are shown in Fig. 5. As shown in the insert, nitrogen coordination leads to deshielding of the ^{113}Cd center, with concomitant resonances of higher chemical shift values. Oxygen coordination produces resonance signals of lower chemical shifts (23). The differences between nitrogen and oxygen coordination are reflected in the comparison of imidazole (175 ppm) and EDTA (108 ppm).

TABLE 1 K_d for OR Histidine ε Nitrogen

	K_d (μM)	Error (μM)
OR histidine Nε2-Hε1	1187	±200
OR histidine Nε2-Hδ2	1253	±245

The top represents OR histidine Nε2-Hε1, and the bottom represents OR histidine Nε2-Hδ2.

All peptide and protein samples gave only a single resonance line consistent with fast exchange between the coordinated species and free Cd^{2+} in buffered solution, as seen with the ^{1}H-^{15}N HSQC above (Fig. 2). A peptide containing the isolated 4-Octa peptide, OR segment (KKRPKP-PrP (56–90)-NH_2) produces a single line with a ^{113}Cd chemical shift close to that of imidazole, consistent with our findings above that Cd^{2+} coordinates primarily through His side chains. Full-length PrP^C is further deshielded relative to the isolated OR by ~5 ppm. Consequently, either the *cis* interaction described above further stabilizes OR-Cd^{2+} coordination or the Cd^{2+} coordination shell is additionally enhanced by C-terminal His residues. To test for this latter case, we prepared PrP^C(H139Y, H176Y), which replaces two C-terminal His residues at the Cd^{2+}-OR docking interface, specifically, H139 on the β1-α1 loop and H176 on α2. The resulting ^{113}Cd spectrum is equivalent to that of wild-type PrP^C, suggesting that either Cd^{2+} remains fully confined by coordination to the OR His residues or that one or two of the C-terminal His residues replace OR His residues thereby maintaining a four-His coordination environment.

To directly test the involvement of Cd^{2+} binding to the flexible N-terminal PrP^C domain, we prepared a mutant in which all OR His residues, His95, and His110 were mutated to Ala. This His-to-Ala mutant shows a strong shift toward a more shielded ^{113}Cd signal of ~35 ppm, close to that of $CdCl_2$ in aq solution. We therefore conclude that, indeed, the N-terminal segment provides the primary coordination environment for Cd^{2+} with a three- or four-His coordination shell, as previously found for Zn^{2+}.

The fast-exchange conditions observed for ^{113}Cd provide an opportunity to estimate the chemical shift of the OR -$^{113}Cd^{2+}$ species. Under fast exchange, the observed signal is a weighted average of the free and fully PrP^C-bound ^{113}Cd chemical shifts. Using a K_d = 1.2 mM determined

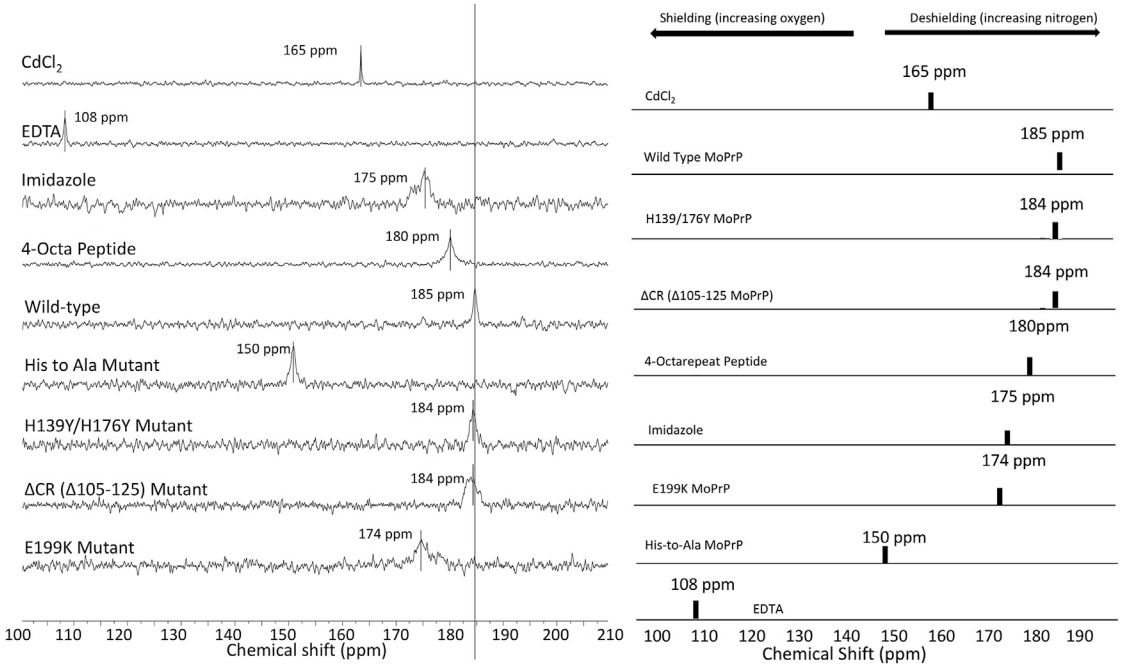

FIGURE 5 ^{113}Cd NMR spectra of controls, octarepeat (OR) segment, full-length PrP^{C}, and relevant mutants. (*left*) ^{113}Cd NMR spectra with chemical shifts referenced to 0.1 M $Cd(ClO_4)_2$ (aq). Spectra for the OR peptide (4-Octa peptide) and all proteins were acquired with 300 μM peptide/protein and 1.0 mM $^{113}Cd^{2+}$. The vertical line is drawn as a reference against wild-type protein. (*right*) A stick diagram of the ^{113}Cd NMR spectra ordered by chemical shift from high to low (with reference $CdCl_2$ at the *top*). As noted at the top, nitrogen coordination decreases chemical shielding, leading to higher chemical shift values, whereas oxygen coordination shifts in the opposite direction.

for the isolated 4-Octa OR segment (peptide concentration = 300 μM and $[Cd^{2+}] = 1.0$ Mm), we calculate that the concentration of the bound OR-Cd^{2+} species is 126 μM or 12.6% of the total $^{113}Cd^{2+}$ in solution. Given the free $^{113}Cd^{2+}$ signal of 165 ppm (from $CdCl_2$) and exchanged average signal of 180 ppm, the fully bound species is determined to be approximately 300 ppm. This value aligns well with published values of 310–320 ppm for superoxide dismutase, which coordinates through a histidine-rich environment (36–38).

Next, we evaluated two important mutants than link directly to prion disease. ΔCR PrP^{C} is a designed deletion mutant in which residues 105–125, corresponding to the central region, are eliminated. Loss of this 21-residue segment between the OR and globular C-terminal domain drives severe cerebellar degeneration and neonatal lethality in laboratory mice (39). Electrophysiological experiments performed on cells transfected with the ΔCR PrP^{C} gene show spontaneous cationic currents associated with the early stages of prion disease (40,41). In cell culture, these currents are inhibited by the addition of Cu^{2+}, which binds with high affinity to the OR (16). Similar to Zn^{2+}, Cu^{2+} drives a *cis* interaction, and previous work from our lab showed a loss of this copper-promoted interaction in ΔCR PrP^{C}. Fig. 5 shows that ΔCR PrP^{C} gives a ^{113}Cd spectrum approximately equivalent to that of wild-type PrP^{C}. Consequently, there is no loss of Cd^{2+} coordination in ΔCR PrP^{C}; however, we cannot rule out a potential loss of the metal-ion-promoted *cis* interaction.

Finally, we examined murine PrP^{C}(E199K), a mutation that corresponds to familial E200K in humans (42,43). Families that carry this fully penetrant E200K mutation develop midlife CJD (44). Spevacek et al. demonstrated that the E199K mutation exhibits a weakened *cis* interaction, relative to wild-type, upon the addition of Zn^{2+} (15). They postulated that because E199 is located on the N-terminal end of helix 3 contributing to a large concentration of negatively charged C-terminal residues, the mutation to a Lys confers toxicity by reducing this localized negative charge thereby weakening electrostatic contributions to the *cis* interaction (15). The ^{113}Cd spectrum of PrP^{C}(E199K) shows a significant shift relative to that obtained from wild-type PrP^{C}, with a chemical shift reflecting a partial loss of nitrogen coordination. Complementing the findings of Spevacek et al. (15), these data suggest partial release of the metal ion.

We next performed ITC measurements on both wild-type PrP^{C} and the E199K mutant to test whether the difference in ^{113}Cd chemical shift arises from a change in metal ion affinity. K_d values were determined for Cd^{2+} and Zn^{2+} binding to both proteins, as well as Zn^{2+} binding to the N-terminal peptide segment (PrP(23–125)). K_d values are reported in Table 2 (ITC curves are in Fig. S2). Wild-type PrP^{C} gives a K_d of ~3.0 mM, in reasonable agreement with 1.2 mM obtained from NMR using the fast exchange approximation (above). Comparing wild-type and mutant PrP^{C}, we find that there is a very slight increase in K_d for Cd^{2+} binding to PrP^{C}(E199K) relative to wild-type PrP^{C}; however, the

TABLE 2 K_d **for** Zn^{2+} **and** Cd^{2+} **Determined by ITC**

	Zn^{2+} K_d (μM)[a]	Cd^{2+} K_d (mM)[a]
Wild-type PrP^C	16.9 ± 1.2	3.0 ± 1.8
PrP^C(E199K)	33.6 ± 0.3	3.3 ± 0.8
N-terminal PrP(23–125)	38.0 ± 0.1	N/A

N/A, not acquired.
[a]Note different units for Zn^{2+} (μM) and Cd^{2+} (mM).

difference is within experimental error. By contrast, the K_d difference for Zn^{2+} shows a factor of two increase for PrP^C(E199K) compared to wild-type PrP^C, thus reflecting a lower affinity for the mutant. In addition, K_d for PrP^C(E199K) is approximately equivalent to that obtained from N-terminal PrP (23–125). Together, these data demonstrate that the C-terminal domain in wild-type PrP^C enhances the OR domain's affinity for Zn^{2+} and that this enhancement is lost in PrP^C(E199K).

To further explore the consequence of the E199K mutation, we performed ^{15}N-^{1}H HSQC NMR in the presence of 1.0 mM $CdCl_2$. Fig. 6 shows that the E199K mutation significantly weakens the observed *cis* interaction relative to wild-type, similar to our previous observations with Zn^{2+}. The majority of the remaining broadened residues are localized to helix 1; line shape broadening of crosspeaks from residues at the respective N-termini of helices 2 and 3 is much less pronounced. Collectively, with the ITC measurements above, these data suggest that residues E199 in the wild-type protein promotes the *cis* interaction and enhances metal ion binding affinity.

DISCUSSION

PrP^C is a Zn^{2+} binding protein, and emerging evidence suggests that uptake of this essential metal ion of the central nervous system drives an intramolecular *cis* interaction that is critical for regulating PrP^C function and arresting inherent toxicity. Previous to this current study, we used chemical mapping performed on an OR peptide to suggest that Zn^{2+} coordinates exclusively to OR His side-chain imidazole groups (10). Here, we used Cd^{2+} as a Zn^{2+} surrogate to carefully investigate the metal ion coordination features and the resulting *cis* interaction. As with Zn^{2+}, ^{1}H-^{15}N HSQC NMR experiments show that the binding of Cd^{2+} to the N-terminal OR segment of PrP^C leads to broadening of select C-terminal residues located to a shallow, negatively charged cleft formed primarily by three α-helices. Next, we used a modified ^{1}H-^{15}N HSQC NMR sequence that selects for $^{2}J_{NH}$ scalar couplings to assess the Cd^{2+}-PrP^C K_d, in turn establishing optimal conditions for ^{113}Cd NMR studies (23,30,31). Finally, ^{113}Cd NMR studies allowed us to compare Cd^{2+} complexation features among the isolated OR, the full-length PrP^C protein, as well as important mutants.

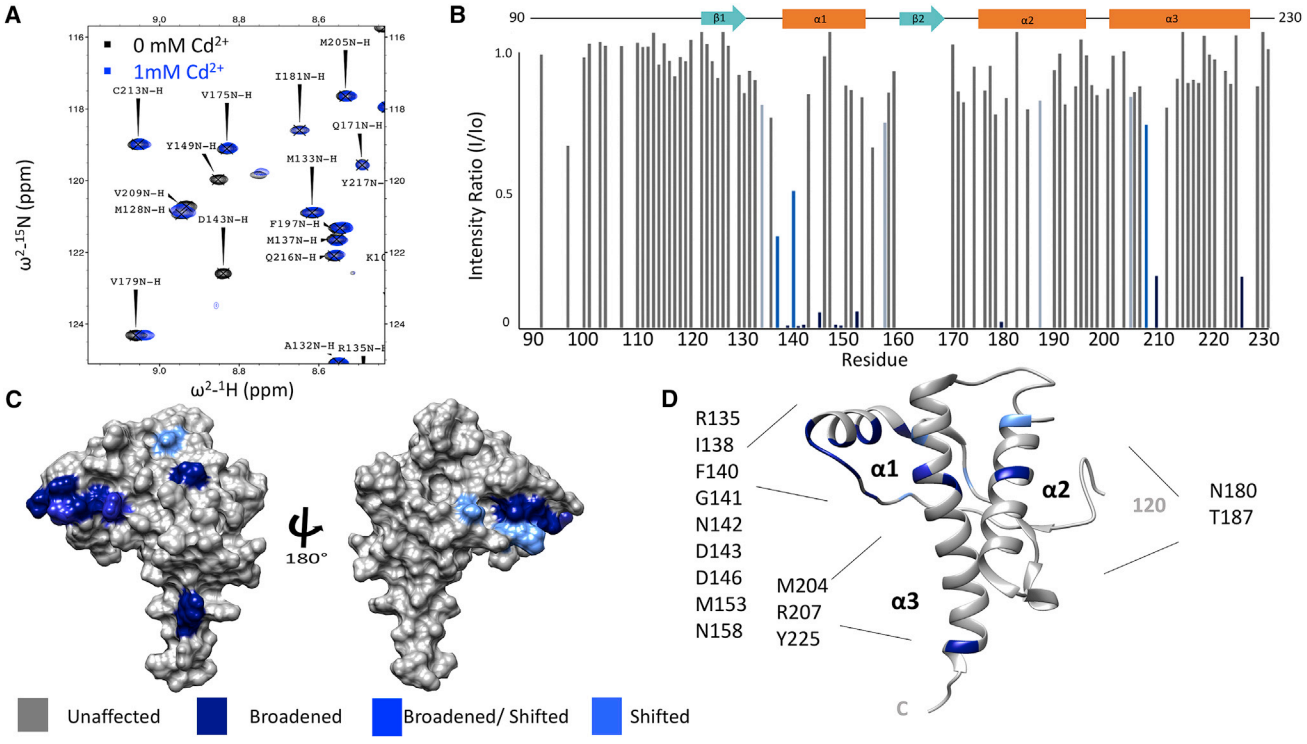

FIGURE 6 Cd^{2+}-promoted interdomain interaction PrP^C(E199K) is significantly weakened relative to the wild-type. The PrP^C mutation E200K (E199K in mouse) correlates with the human prion CJD. (*A*) A selected region of the ^{1}H-^{15}N HSQC of wild-type PrP in the absence of metal (*black*) and in the presence of 1.0 mM of Cd^{2+} (*blue*). (*B*) A bar graph of I/I_o for residues 90–23 of PrP^C in the presence of Cd^{2+}. (*C* and *D*) Surface and ribbon plots, respectively, of C-terminal residues affected by the presence of Cd^{2+} (coordinates from PDB: 1XYX). Affected residues are noted specifically on the ribbon diagram.

Given the remarkable chemical shift sensitivity of ^{113}Cd, the agreement between the isolated OR and the full-length protein provides strong evidence that the OR alone is responsible for direct Cd^{2+} coordination (23). Consistent with this proposal, elimination of N-terminal His residues leads to a significant change in ^{113}Cd chemical shift. Moreover, analysis of the fast-exchange signal finds a calculated chemical shift of the Cd^{2+}-PrP^C species to be consistent with coordination by three- or four-His nitrogen atom configuration (35,45). Together, these findings with Cd^{2+} as a surrogate support our previous proposal that PrP^C takes up Zn^{2+} with three- or four-His coordination in the repeat domain.

After our chemical mapping studies (10), several extended x-ray absorption fine-structure (EXAFS) and related x-ray studies investigated Zn^{2+} coordination to PrP^C (46,47). Stellato et al. probed the competition between Zn^{2+} and Cu^{2+} coordination and showed that at low Cu^{2+} occupancy, Zn^{2+} partially displaces His side chains from the copper centers (48). In a separate study, this group found that Zn^{2+} does not fully coordinate to all OR His residues but instead may facilitate OR peptide clustering (47). Given that this work was performed exclusively on OR peptides, it is not clear whether this type of metal ion-assisted cross-linking applies to full-length PrP^C. Pushie et al. (46) combined density functional theory and EXAFS to carefully examine Zn^{2+} occupation of the OR. Interestingly, their calculations found little energy difference between Zn^{2+} coordinated to three imidazole groups and a single water versus Zn^{2+} coordinated to four imidazoles. This finding was supported by analysis of the EXAFS data, which were well fit with a model of only three imidazole groups (46). Our findings here suggest three- or four-His coordination as determined by extrapolation from the fast-exchange signal and comparison of the estimated chemical shift to that of known His-rich Cd^{2+} complexes. As such, our result, although an approximation, is consistent with the findings of Pushie et al. (46).

A surprising finding of our study is the significant change in chemical shift associated with the E199K mutation. In humans, the parallel E200K mutation potently confers familial CJD (44,49). Residue 200 is located near the N-terminal end of α3, so it is therefore reasonable to hypothesize that this mutation destabilizes the protein thereby promoting aggregation (6). However, biophysical studies with NMR and circular dichroism find that PrP^C(E200K) maintains the same fold and stability as the wild-type protein (15,50,51). Residue E200 contributes to a highly conserved, negatively charged electrostatic patch on the PrP^C C-terminal domain (15). In our previous investigations with PrP^C-Zn^{2+} binding, we noted that all C-terminal disease promoting mutations involving acidic or basic residues results in a reduction of the patch's negative charge character. Using ^{1}H-^{15}N HSQC NMR, we directly tested the influence of the Glu→Lys mutation and found a significant loss of the Zn^{2+}-promoted *cis* interaction, especially in the vicinity of α3 (15). This finding led to the proposal of a new paradigm for understanding the E200K and related mutations in which alteration of the protein's electrostatics results in a weakening of the regulatory *cis* interaction. Our findings here take this concept further by suggesting a loss of metal ion affinity. Testing this directly with ITC indeed shows that the affinity for Zn^{2+} is reduced by the Glu→Lys mutation, consistent with the change in ^{113}Cd chemical shift found for PrP^C(E199K) possibly from a loss of nitrogen coordination.

Integrating the observations above suggests a new scheme for understanding the role of residue E200 in stabilizing the PrP^C *cis* interaction. The ^{113}Cd NMR spectra comparing wild-type PrP^C with the OR peptide reflects little change in the metal ion coordination environment. However, mutation to Lys causes a loss of the observed PrP^C *cis* interaction promoted by either Zn^{2+} or Cd^{2+}. These findings may be explained by proposing that E200 contributes to the second coordination sphere of the metal ion. Previous work by Spevacek et al. (15) used molecular dynamics simulations with distance restraints from DEER EPR to localize the OR-Zn^{2+} domain relative to the interfacial binding surface of the C-terminal domain. Inspection of the coordinates from these simulations finds that the side-chain carboxylate of E200 is within hydrogen bonding distance of an imidazole ring NH opposite to the nitrogen that coordinates Zn^{2+}, as shown in Fig. 1. In this paradigm, the mutation E200K does not destabilize the C-terminal domain; instead mutation of the acidic glutamate results in the loss of a Glu-His hydrogen bond that is essential for regulating the otherwise toxic PrP^C N-terminal executive domain.

In summary, ^{113}Cd NMR has provided new and important insights into metal ion coordination in the PrP. Our studies continue to support the concept of an interdomain *cis* interaction promoted by coordination of Zn^{2+} to the OR; mutations that weaken this interaction correlate with inherited prion disease. This concept may prove useful in the continued study of PrP^C function and treatment of prion diseases.

SUPPORTING MATERIAL

Two figures are available at http://www.biophysj.org/biophysj/supplemental/S0006-3495(19)30021-9.

AUTHOR CONTRIBUTIONS

K.A.M. and G.L.M. designed the experiments. K.A.M., G.P.R., R.B.L., and H.-W.L. performed the experiments. K.A.M. and G.L.M. wrote the manuscript. K.A.M., G.P.R., and G.L.M. edited the manuscript.

ACKNOWLEDGMENTS

The authors extend their sincere gratitude to professor Ian M. Armitage, University of Minnesota, for helpful advice on the use of ^{113}Cd as an

NMR probe of metal ion coordination centers and to Kevin Schilling, University of California, Santa Cruz, who generously contributed protein for ^{113}Cd NMR studies. We further thank Dr. Mark Swanson, PhD, San Francisco State University NMR Facility Manager, for help with acquisition of ^{113}Cd spectra.

This work was funded by National Institutes of Health instrumentation grant S10OD018455, which supported acquisition of the University of California, Santa Cruz 800 MHz NMR spectrometer, and National Institutes of Health research grant R01GM065790 (awarded to G.L.M.). The San Francisco State University NMR instrument was supported by National Science Foundation Major Research Instrumentation grant DBI1625721.

REFERENCES

1. Prusiner, S. 1982. Novel proteinaceous infectious particles cause scrapie. *Science.* 216:136–144.
2. Prusiner, S. B. 1997. Prion diseases and the BSE crisis. *Science.* 278:245–251.
3. Herms, J., T. Tings, …, H. Kretzschmar. 1999. Evidence of presynaptic location and function of the prion protein. *J. Neurosci.* 19:8866–8875.
4. Steele, A. D., S. Lindquist, and A. Aguzzi. 2007. The prion protein knockout mouse: a phenotype under challenge. *Prion.* 1:83–93.
5. Millhauser, G. L. 2007. Copper and the prion protein: methods, structures, function, and disease. *Annu. Rev. Phys. Chem.* 58:299–320.
6. Evans, E. G., M. J. Pushie, …, G. L. Millhauser. 2016. Interaction between prion protein's copper-bound octarepeat domain and a charged C-terminal pocket suggests a mechanism for N-terminal regulation. *Structure.* 24:1057–1067.
7. Evans, E. G. B., and G. L. Millhauser. 2017. Copper- and zinc-promoted interdomain structure in the prion protein: a mechanism for autoinhibition of the neurotoxic N-terminus. *Prog. Mol. Biol. Transl. Sci.* 150:35–56.
8. Aronoff-Spencer, E., C. S. Burns, …, G. L. Millhauser. 2000. Identification of the Cu2+ binding sites in the N-terminal domain of the prion protein by EPR and CD spectroscopy. *Biochemistry.* 39:13760–13771.
9. Chattopadhyay, M., E. D. Walter, …, G. L. Millhauser. 2005. The octarepeat domain of the prion protein binds Cu(II) with three distinct coordination modes at pH 7.4. *J. Am. Chem. Soc.* 127:12647–12656.
10. Walter, E. D., D. J. Stevens, …, G. L. Millhauser. 2007. The prion protein is a combined zinc and copper binding protein: Zn2+ alters the distribution of Cu2+ coordination modes. *J. Am. Chem. Soc.* 129:15440–15441.
11. Donne, D. G., J. H. Viles, …, H. J. Dyson. 1997. Structure of the recombinant full-length hamster prion protein PrP(29-231): the N terminus is highly flexible. *Proc. Natl. Acad. Sci. USA.* 94:13452–13457.
12. Brown, L. R., and D. A. Harris. 2003. Copper and zinc cause delivery of the prion protein from the plasma membrane to a subset of early endosomes and the Golgi. *J. Neurochem.* 87:353–363.
13. Watt, N. T., H. H. Griffiths, and N. M. Hooper. 2013. Neuronal zinc regulation and the prion protein. *Prion.* 7:203–208.
14. Watt, N. T., D. R. Taylor, …, N. M. Hooper. 2012. Prion protein facilitates uptake of zinc into neuronal cells. *Nat. Commun.* 3:1134.
15. Spevacek, A. R., E. G. Evans, …, G. L. Millhauser. 2013. Zinc drives a tertiary fold in the prion protein with familial disease mutation sites at the interface. *Structure.* 21:236–246.
16. Wu, B., A. J. McDonald, …, D. A. Harris. 2017. The N-terminus of the prion protein is a toxic effector regulated by the C-terminus. *eLife.* 6:e23473.
17. McDonald, A. J., B. Wu, and D. A. Harris. 2017. An inter-domain regulatory mechanism controls toxic activities of PrP^{C}. *Prion.* 11:388–397.
18. Cotton, F. A., and G. Wilkinson. 1988. Advanced Inorganic Chemistry: A Comprehensive Text. Wiley, New York.
19. Otvos, J. D., I. M. Armitage, …, J. E. Coleman. 1979. 31P NMR of alkaline phosphatase. Dependence of phosphate binding stoichiometry on metal ion content. *J. Biol. Chem.* 254:4707–4713.
20. Armitage, I. M., R. T. Pajer, …, J. E. Coleman. 1976. Cadmium-113 Fourier transform nuclear magnetic resonance of cadmium(II) carbonic anhydrases and cadmium(II) alkaline phosphatase. *J. Am. Chem. Soc.* 98:5710–5712.
21. Jonsson, N. B., L. A. Tibell, …, J. L. Sudmeier. 1980. Cadmium-113 NMR of carbonic anhydrases: effect of pH, bicarbonate, and cyanide. *Proc. Natl. Acad. Sci. USA.* 77:3269–3272.
22. Armitage, I. M., A. J. Schoot Uiterkamp, …, J. E. Coleman. 1978. 113Cd NMR as a probe of the active sites of metalloenzymes. *J. Magn. Reson.* 29:375–392.
23. Armitage, I. M., T. Drakenberg, and B. Reilly. 2013. Use of (113)Cd NMR to probe the native metal binding sites in metalloproteins: an overview. *Met. Ions Life Sci.* 11:117–144.
24. Armitage, I. M., J. D. Otvos, …, Y. Boulanger. 1982. Structure elucidation of the metal-binding sites in metallothionein by 113Cd NMR. *Biophys. Biochem.* 13:2974–2980.
25. Armitage, I. M., and Y. Boulanger. 1983. Cadmium-113 NMR. *NMR New. Access. Nucl.* 2:337–365.
26. Maciel, G. E., and M. Borzo. High resolution l13Cd nuclear magnetic resonance by pulse Fourier transform. *J. Chem. Soc., Chem. Commun.* 19:394a.
27. Kostelnik, R. J., and A. A. Bothner-By. 1974. Cadmium-113 nuclear magnetic resonance studies of cadmium(II)ligand binding in aqueous solutions. I. The effect of diverse ligands on the cadmium-113 chemical shift. *J. Magn. Reson.* 14:141–151.
28. Cardin, A. D., P. D. Ellis, …, J. W. Howard. 1975. Cadmium-113 Fourier transform nuclear magnetic resonance spectroscopy. *J. Am. Chem. Soc.* 97:1672–1679.
29. Lambert, J. B., and F. G. Riddell. 1982. The Multinuclear Approach to NMR Spectroscopy. D. Reidel Publishing Company, Hingham, MA.
30. Pelton, J. G., D. A. Torchia, …, S. Roseman. 1993. Tautomeric states of the active-site histidines of phosphorylated and unphosphorylated IIIGlc, a signal-transducing protein from Escherichia coli, using two-dimensional heteronuclear NMR techniques. *Protein Sci.* 2:543–558.
31. Tettamanzi, M. C., C. Keeler, …, M. E. Hodsdon. 2008. Analysis of site-specific histidine protonation in human prolactin. *Biochemistry.* 47:8638–8647.
32. Raran-Kurussi, S., S. Cherry, …, D. S. Waugh. 2017. Removal of affinity tags with TEV protease. *Methods Mol. Biol.* 1586:221–230.
33. Delaglio, F., S. Grzesiek, …, A. Bax. 1995. NMRPipe: a multidimensional spectral processing system based on UNIX pipes. *J. Biomol NMR.* 6:277–293.
34. Pettersen, E. F., T. D. Goddard, …, T. E. Ferrin. 2004. UCSF Chimera–a visualization system for exploratory research and analysis. *J. Comput. Chem.* 25:1605–1612.
35. Williamson, M. P. 2013. Using chemical shift perturbation to characterise ligand binding. *Prog. Nucl. Magn. Reson. Spectrosc.* 73:1–16.
36. Marchetti, P. S., M. A. Kennedy, …, T. W. Bell. 1989. Cadmium-113 NMR spectroscopy. Long bond interactions and chemical shielding in the cadmium complex of an unsaturated nitrogen analogue of 18-crown-6. *J. Am. Chem. Soc.* 111:2063–2066.
37. Bailey, D. B., P. D. Ellis, and J. A. Fee. 1980. Cadmium-113 nuclear magnetic resonance studies of cadmium-substituted derivatives of bovine superoxide dismutase. *Biochemistry.* 19:591–596.
38. Kofod, P., R. Bauer, …, M. J. Bjerrum. 1991. ^{113}Cd-NMR investigation of a cadmium-substituted copper, zinc-containing superoxide dismutase from yeast. *Eur. J. Biochem.* 8:607–611.
39. Li, A., H. M. Christensen, …, D. A. Harris. 2007. Neonatal lethality in transgenic mice expressing prion protein with a deletion of residues 105-125. *EMBO J.* 26:548–558.
40. Solomon, I. H., N. Khatri, …, D. A. Harris. 2011. An N-terminal polybasic domain and cell surface localization are required for mutant prion protein toxicity. *J. Biol. Chem.* 286:14724–14736.

41. Biasini, E., J. A. Turnbaugh, …, D. A. Harris. 2012. The toxicity of a mutant prion protein is cell-autonomous, and can be suppressed by wild-type prion protein on adjacent cells. *PLoS One.* 7:e33472.

42. Bell, J. E., and J. W. Ironside. 1993. Neuropathology of spongiform encephalopathies in humans. *Br. Med. Bull.* 49:738–777.

43. Kong, Q., W. K. Surewicz, …, P. Montagna. 2008. Inherited prion diseases. *In* Prion Diseases and Biology. S. B. Prusiner, ed. Cold Spring Harbor Laboratory Press, pp. 673–775.

44. Mead, S. 2006. Prion disease genetics. *Eur. J. Hum. Genet.* 14:273–281.

45. Borsari, M. 2014. Cadmium: coordination chemistry. Encyclopedia of Inorganic and Bioinorganic Chemistry. John Wiley & Sons, Ltd., pp. 1–16.

46. Pushie, M. J., K. H. Nienaber, …, G. N. George. 2014. Combined EXAFS and DFT structure calculations provide structural insights into the 1:1 multi-histidine complexes of Cu(II), Cu(I), and Zn(II) with the tandem octarepeats of the mammalian prion protein. *Chemistry.* 20:9770–9783.

47. Stellato, F., V. Minicozzi, …, S. Morante. 2014. Copper-zinc cross-modulation in prion protein binding. *Eur. Biophys. J.* 43:631–642.

48. Stellato, F., A. Spevacek, …, S. Morante. 2011. Zinc modulates copper coordination mode in prion protein octa-repeat subdomains. *Eur. Biophys. J.* 40:1259–1270.

49. Minikel, E. V., S. M. Vallabh, …, D. G. MacArthur. 2016. Quantifying prion disease penetrance using large population control cohorts. *Sci. Transl. Med.* 8:322ra9.

50. Bae, S. H., G. Legname, …, H. J. Dyson. 2009. Prion proteins with pathogenic and protective mutations show similar structure and dynamics. *Biochemistry.* 48:8120–8128.

51. Liemann, S., and R. Glockshuber. 1999. Influence of amino acid substitutions related to inherited human prion diseases on the thermodynamic stability of the cellular prion protein. *Biochemistry.* 38:3258–3267.

Biophysical Journal, Volume *116*

Supplemental Information

Molecular Features of the Zn^{2+} Binding Site in the Prion Protein Probed by ^{113}Cd NMR

Kate A. Markham, Graham P. Roseman, Richard B. Linsley, Hsiau-Wei Lee, and Glenn L. Millhauser

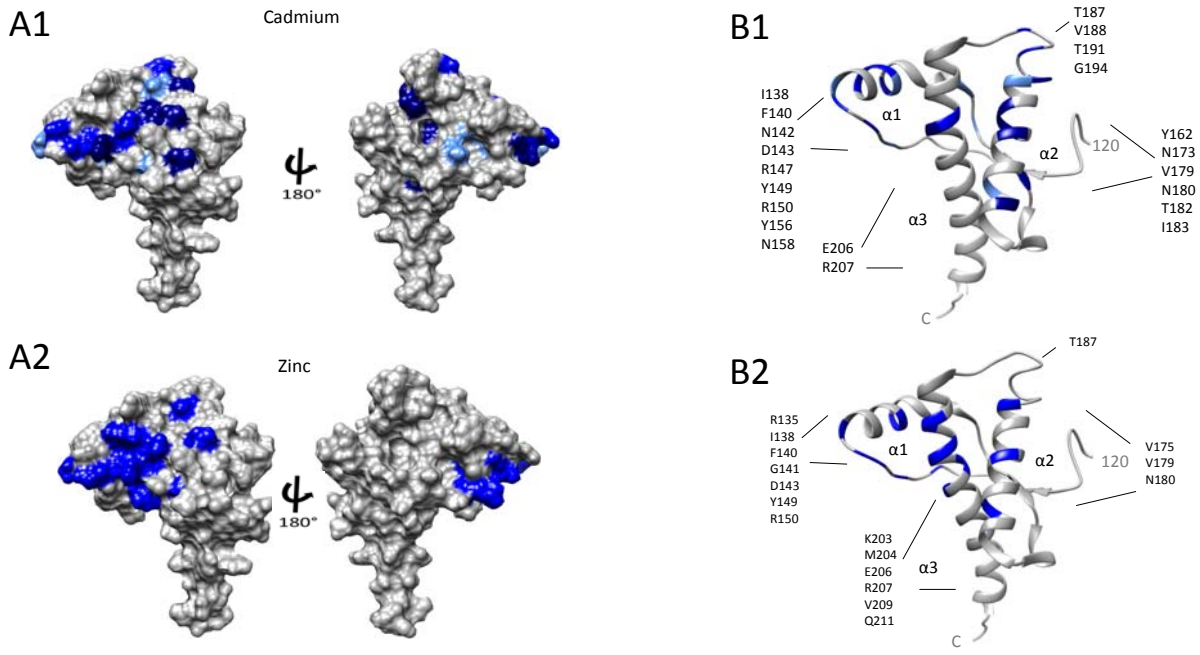

Figure S1 Zn^{2+} and Cd^{2+} Promoted *cis* Interaction Wild-Type MoPrP is Localized to the Same C-terminal Surface. Both samples were run with 300μM protein in a buffer containing 10mM MES (Sigma), 10% D_2O, at pH 7.0 for solubility purposes. Subsequent to the addition of 500μM $ZnCl_2$ or 1mM $CdCl_2$, the pH was measured and adjusted, if necessary. Residues that are broadened (dark blue), broadened+shifted (medium blue), and shifted (light blue) in the presence of the respective metal ion are indicated in the surface diagrams, A1 and A2, and ribbon diagrams, B1 and B2. Coordinates for the C-terminal PrP^C structure are from PDB:1XYX.

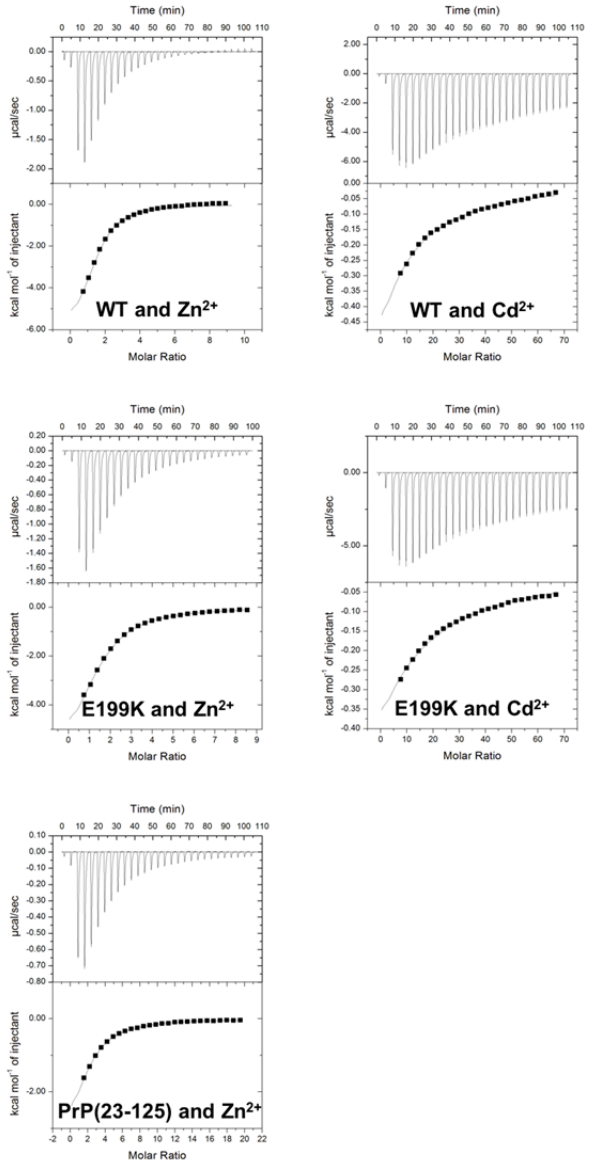

Figure S2 Raw isotherms of either Zn^{2+} or Cd^{2+} ITC titrations into different PrP^{C}variants: Zinc Chloride (2 mM) or Cadmium Chloride (20 mM) was titrated into PrP^{C}variants. Each figure contains the raw ITC data (top panel) and the integrated raw data (bottom panel). Zinc chloride was titrated into WT, E199K, and PrP(23-125) at pH 7.4 in 50 mM MOPS buffer. Cadmium chloride was titrated into WT and E199K at pH 6.0 in 10 mM MES buffer. The integrated raw ITC data shown for cadmium chloride have been background subtracted due to high heats of dilution. Calculated Kd values are reported in Table 2.